Magnetic Properties of 1D Iron–Sulfur Compounds Formed Inside Single-Walled Carbon Nanotubes

Okotrub Alexander V., Chernov Alexander I., Lavrov Alexander N., Gurova Olga A., Shubin Yury V., Palyanov Yuri N., Borzdov Yuri M., Zvezdin Anatoly K., Lähderanta Erkki, Bulusheva Lyubov G., Sedelnikova Olga V.

DOI: 10.1002/pssr.202000291

Magnetic properties of one-dimensional iron-sulfur compounds formed inside single-walled carbon nanotubes

A.V. Okotrub,[1] A.I. Chernov,[2,3*] A.N. Lavrov,[1] O.A. Gurova,[1] Yu.V. Shubin,[1] Yu.N. Palyanov,[4,5] Yu.M. Borzdov,[5] A.K. Zvezdin,[3,6] E. Lähderanta,[7] L.G. Bulusheva,[1] O.V. Sedelnikova[1*]

[1]*Nikolaev Institute of Inorganic Chemistry, SB RAS, 3 Acad. Lavrentiev Ave., 630090, Novosibirsk, Russia*
[2]*Russian Quantum Center, Skolkovo innovation city, 30 Bolshoy Bulvar, 121205, Moscow, Russia*
[3]*Center for Photonics and 2D Materials, Moscow Institute of Physics and Technology (National Research University), 9 Institutskiy per., 141700, Dolgoprudny, Russia*
[4]*Novosibirsk State University, 2 Pirogova Str., 630090, Novosibirsk, Russia*
[5]*Sobolev Institute of Geology and Mineralogy, SB RAS, 3 Acad. Koptyug Ave. 3, 630090, Novosibirsk, Russia*
[6]*General Physics Institute, 38 Vavilov Str., 119991, Moscow, Russia*
[7]*LUT-University, 53850 Lappeenranta, Finland*

Abstract

In this work, we perform the filling of single-walled carbon nanotubes (SWCNTs) with sulfur and study the magnetic properties of the formed nanomaterials. Encapsulation of sulfur species results in the appearance of a specific magnetic ordering in the system due to the formation of nanoscopic grains composed of sulfur and residual catalytic Fe nanoparticles contained in the SWCNTs. We study the magnetic character of the obtained 1D nanostructures using SQUID magnetometer and reveal a sequential ferromagnetic-antiferromagnetic ordering in the material. Magnetic and optical properties are strongly dependent on the synthesis protocols. We obtain a significant Raman intensity increase related to the encapsulated nanostructures when filling is performed at high-pressure high-temperature conditions. Simultaneously, the magnetic susceptibility gets strongly reduced for high-pressure filling which is related to the escape of iron particles from the nanotube interior, and the magnetic properties of the material are governed by a weak ferromagnetic ordering of Fe-S structures remained inside SWCNTs. Sulfur encapsulation provides the new route for controlling the magnetic properties in 1D nanomaterials that pave the way for advanced magnetooptical applications.

Text

Carbon-encapsulated magnetic nanoparticles are very prospective in the context of biomedical applications [1], memory devices [2], and magnetic sensors [3]. Single-walled carbon nanotubes (SWCNTs) stand out among other different protective materials. They not only serve as a template for nano-dimensional growth [4] and promote interactions between the encapsulated species, but also can influence the properties of the formed host-guest structures [5,6,7]. Indeed, the SWCNT ensures a fine dispersion of magnetic species along the longitudinal axis thus restricting the magnetic coupling between them and thereby enhancing the inherent properties of nanoparticles [8–11]. A reduction of intermolecular dipole-dipole interactions between the neighboring encapsulated molecules leading to enhanced magnetic properties was recently demonstrated for single-molecule magnets [12]. 1D arrangement of single-molecule magnets provides the suppression

This article has been accepted for publication and undergone full peer review but has not been through the copyediting, typesetting, pagination and proofreading process, which may lead to differences between this version and the Version of Record. Please cite this article as doi: 10.1002/pssr.202000291.

of quantum tunneling of the magnetization [12,13] that is crucial for practical applications. Initially, filling of nanotubes with magnetic species was studied for cobalt [8,14,15], iron [9,10,16,17,18] and nickel [19] nanoparticles. These metals are frequently used as catalysts for the growth of nanotubes [20], and often detected as side products even after the purification process [21]. Briones-Leon *et al.* [22] specifically studied the effects coming from iron filling of SWCNTs differed by the type of conductivity. It was revealed that magnetic properties are affected by both the metallicity and the diameter of nanotubes, encapsulating nanoclusters of different sizes. Namely, the iron-filled metallic SWCNTs demonstrated the pronounced ferromagnetic behavior, while the semiconducting ones were paramagnetic. It is worth noting that magnetic moments associated with structural defects in pristine, non-filled SWCNTs can also order ferromagnetically with the transition temperature being higher in metallic tubes than in semiconducting ones due to the spin-spin interaction via conduction electrons [23,24].

Recently, sulfur confined inside SWCNTs has attracted a lot of much attention [25,26]. Researchers focus, in particular, on the study of the chemical properties of the encapsulated material and the identification of chemical reactions with lithium ions in order to improve the performance of batteries [26]. Interaction of iron and sulfur can lead to formation of various functional materials, whereas the confinement provides improvement of properties required for solar energy conversion based on iron pyrite [27], electrode materials for lithium-ion batteries [28,29] or applications based on hydrogen evolution reactions [30].

Iron-sulfur compounds include a rich diversity of phases with various magnetic properties that make them very attractive for filling of SWCNTs. Conventional synthesis of Fe – S compounds in bulk results in various products including mackinawite (tetragonal FeS), cubic FeS, troilite (hexagonal FeS), pyrrhotite ($Fe_{1-x}S$), greigite (cubic Fe_3S_4), pyrite (cubic FeS_2), and marcasite (orthorhombic FeS_2). Both forms of bulk FeS_2 are non-magnetic. In pyrite, Fe^{2+} ions are in a low spin state leading to a diamagnetic response [31]. At the same time, $Fe_{1-x}S$ materials (x=0-0.2) exhibit magnetic ordering. Iron-rich structures could be ferromagnetic (hexagonal FeS [32]), antiferromagnetic (expanded tetragonal FeS [33] and monoclinic $Fe_{1-x}S$ [34]) or ferrimagnetic (Fe_3S_4 and $Fe_{1-x}S$ [35]). The magnetic ordering of iron sulfides depends on crystallinity, the presence of sulfur vacancies [36,37], impurity phases (*i.e.*, Co doping), and particle size in the nanometer regions [38]. All these factors can lead to a modified magnetic response. Implementation of SWCNTs with known diameters can provide a model structure for studying the properties of ordered magnetic nanomaterial. One of the routes for construction of iron sulfide structures inside the nanotubes is the use of metallic nanograins that are located inside the nanotube channels due to the growth protocols and encapsulation of sulfur through the vapor phase. The properties of resulting iron-sulfur structures may exhibit dependence not only on their particular arrangement and composition, but also on the charge transfer between the encapsulated species and nanotube walls.

In this work, we investigate the magnetic properties of nanoscopic iron-sulfur grains synthesized inside of SWCNTs from encapsulated sulfur and residual iron that was initially used to catalyze the growth of these SWCNTs. We compare the morphology, composition and magnetic properties of products obtained by heating a mixture of SWCNTs with sulfur under high-temperature (HT) and high-temperature high-pressure (HTHP) conditions. In the former case, it is shown that along with sulfur, nanotubes contain encapsulated pyrite nanoparticles, which ensure the antiferromagnetic response of the host-guest nanostructures. The material obtained under HTHP conditions consists of SWCNTs tightly filled with sulfur as indicated by the giant Raman response from the encapsulated species. However, high pressure applied to a mixture of SWCNTs and sulfur along with the heating significantly deforms nanotubes and results in the reconfiguration of the inner structure and escape of the majority of large magnetic particles from the nanotubes thereby quenching the magnetic response of the material.

Experiments were performed on commercially available SWCNTs (TUBALL™, OCSiAl, Novosibirsk) with an average diameter distribution of 1.7-1.9 nm. In order to remove amorphous carbon and residual external catalyst nanoparticles composed mainly from Fe (~7 wt%), SWCNTs were purified using the procedure described elsewhere [21]. The remaining Fe content in the purified

SWCNTs was estimated by atomic absorption spectroscopy (AAS) to be about 0.3 wt%. These nanotubes were continuously heated with sulfur in a sealed ampoule (HT method) followed by the toluene treatment to remove sulfur from the outside

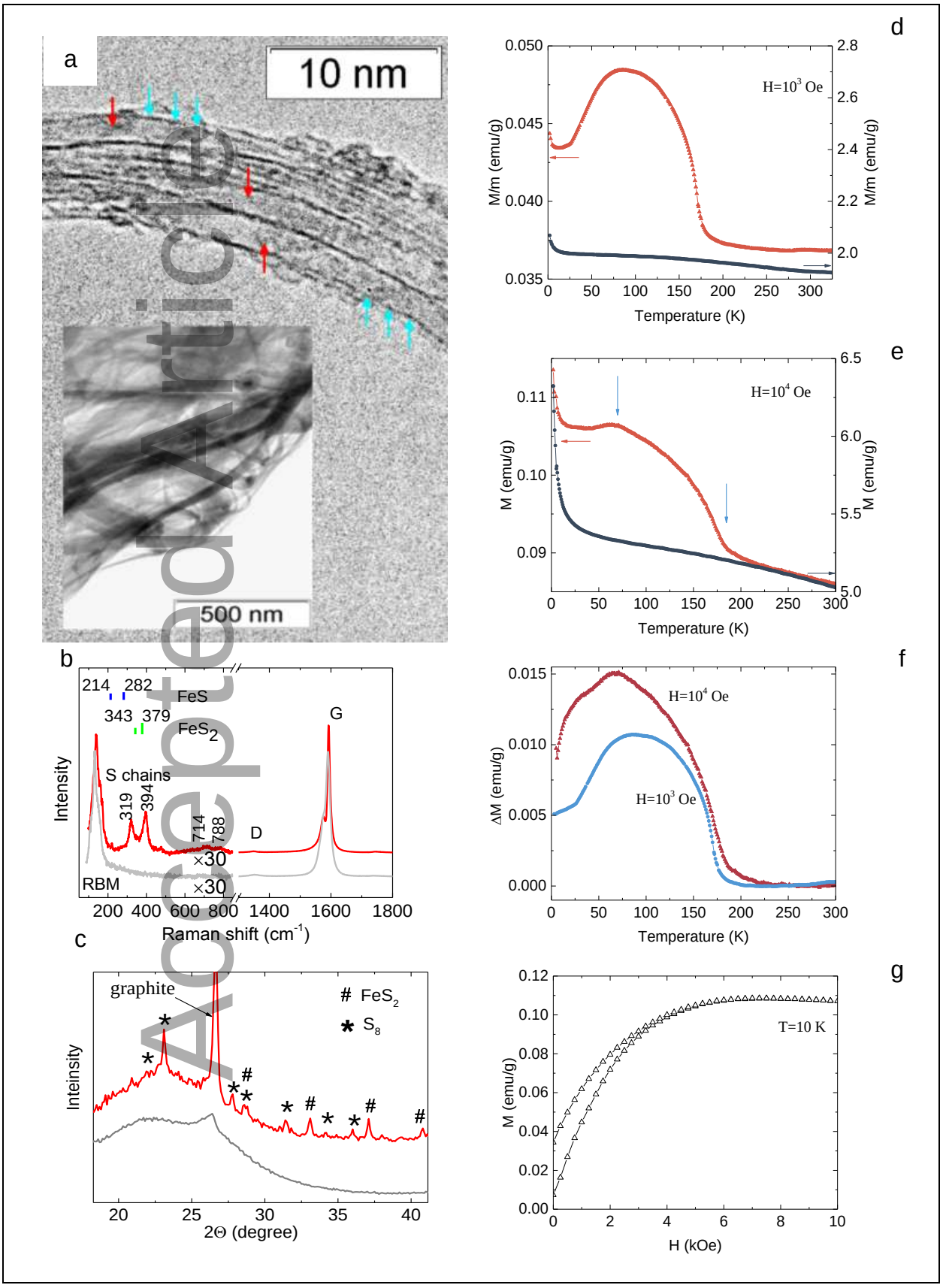

Figure 1. SWCNTs filled with sulfur under high temperature: (a) HR TEM image (cyan and red arrows indicate SWCNTs' walls and sulfur chains), insert shows TEM image, (b) Raman spectra (spectra in low-wave number region (b) are multiplied by factor 30) and (c) XRD patterns for pristine (grey) and sulfur-filled (red) SWCNTs, (d) ZFC magnetization data for pristine (grey) and sulfur-filled (red) SWCNTs at H = 1 kOe and (e) at H = 10 kOe, (f) sulfur-related magnetization contribution determined by subtracting a scaled magnetization of pristine SWCNTs from the magnetization of sulfur-filled SWCNTs. Note the field-independent starting temperature of the additional ferromagnetic response and the shift of the magnetization decrease with increasing magnetic field. (g) Hysteresis M (H) curve measured at 10 K.

of the nanotubes, while the sulfur located inside the nanotubes remained intact [39]. Energy dispersive X-ray (EDX) spectroscopy revealed ca. 12.7 wt% of sulfur, the content of iron estimated by AAS was about 0.3 wt%. Due to a quite low iron concentration, its visualization using microscopy methods is a rather challenging task. However, sulfur chains placed inside the SWCNTs are discernible in the high-resolution transmission electron microscopy (HR TEM) images (indicated by red arrows in Figure 1a). The homogeneous filling of nanotubes with sulfur by the ampoule method was also previously demonstrated [39]. Both TEM and Raman spectra have shown that SWCNTs filled with sulfur keep their integrity (Figure 1a,b); no metallic particles can be seen. However, when sulfur is filling the SWCNTs that contain encapsulated residual iron catalyst, iron sulfides are also expected to be formed [39] as confirmed by X-ray diffraction (XRD) analysis (Figure 1c). One can see the pattern of pyrite FeS_2, which is one of the most probable compounds to be formed according to the iron-sulfur phase diagram [40]. Note that the fingerprint from graphite is due to graphite foil used to prepare the sample for the XRD study. However, Raman spectroscopy identifies mostly the spectral peaks related to sulfur chains [41] while no considerable response from pyrite or Fe related vibrations [42] is seen (vibrations of FeS [43] and FeS_2 [44] are shown by bars), making the evaluation of the specific structure of the encapsulated material challenging. One of the ways to detect the Raman signal should be in using different excitation wavelengths in order to resonantly excite the inner structure, similarly to the case of graphene nanoribbons inside SWCNTs [45].

Figure 1d,e shows the SQUID magnetization data for sulfur-filled SWCNTs in comparison with those for the sulfur-free purified SWCNTs. For the sulfur-free SWCNTs, we detect a weak ferromagnetic response at temperatures at least up to 330 K – a contribution originating from iron encapsulated in nanotubes, which accompanies the intrinsic diamagnetic response of SWCNTs. This behavior is similar to the results reported for iron-filled SWCNTs [46]. According to the magnetization value, the iron content is estimated as ~0.5 wt% which reasonably agrees with the value obtained by AAS method. Filling the nanotubes with sulfur results in a drastic change of magnetic properties. The magnetization significantly decreases for the filled samples, by about an order of a magnitude in the temperature range 175 – 330 K. Above 175 K the scaled temperature dependence of magnetization well match that of sulfur-free nanotubes, while an additional pronounced feature appears at temperatures below 175 K. It can be seen explicitly after the subtraction of the background related to pristine SWCNTs and encapsulated Fe nanoparticles (Figure 1f). Note, that the magnetization curve of sintered sulfur is featureless in this temperature region (Supporting Figure 1). When temperature decreases, the magnetization of sulfur-filled SWCNTs grows significantly reaching maximum values around 75 K with further continuous decrease at temperatures below 50 K. We identify two characteristic temperatures marked with blue arrows in Figure 1e. The higher one being about 175 K marks the inception of the magnetization increase that we attribute to the formation of ferromagnetic response of encapsulated sulfur-containing nanostructures. The second one (~75 K) corresponds roughly to the point where the magnetization reaches its local maximum, thus indicating where an additional magnetic ordering mechanism starts to be pronounced. At 75 K the impact of external magnetic field on encapsulated ferromagnetic nanoclusters is apparently exceeded by the magneto-dipole or antiferromagnetic-type exchange interaction between the nanoclusters. This results in the appearance of antiferromagnetic

ordering, which prevails at temperature below ~75 K. The magnetization peak position shifts towards lower temperatures with increasing magnetic field (Figure 1f), since stronger antiferromagnetic interactions are needed to override the external field influence. Rather broad features in the M(T) dependences can be explained by the distribution in size and also geometry of the encapsulated nanostructures and therefore different Curie temperatures due to finite-size effects [47]. The observed peculiar magnetic ordering is apparently produced by the nanostructures formed due to the reaction of residual Fe nanoparticles with sulfur inside SWCNTs.

An examination of the M(H) curve at 10 K (Figure 1g) reveals that ferromagnetic fragments partially survive down to low temperatures providing the magnetic irreversibility and considerable remnant magnetization. It is worth noting also that the sample's magnetization saturates at rather low field of about 5 kOe giving an additional evidence for fairly large correlated nanoparticles. Given the possible size of encapsulated particles and the observed coercive field, one can infer that ferromagnetic nanoparticles should possess a monodomain state [48, 49], while the relative arrangements of their moments is governed by an external field and interactions within the host-guest structure.

As we mentioned above, iron-sulfur compounds exhibit very different magnetic responses including antiferromagnetic ordering for FeS and $Fe_{1-x}S$. However, our XRD data have revealed the patterns only from non-magnetic pyrite. In order to understand the morphology of iron sulfide synthesized inside nanotubes, we performed a control experiment of sintering iron with sulfur excess (1:2) in the same conditions as when filling the SWCNTs. The Raman spectrum for this sulfide exhibits the vibrations characteristic of pyrite FeS_2 (Supporting Figure 2). However, the magnetization curves measured upon heating after zero-field cooling and field cooling both demonstrate a complicated magnetic response and give an additional understanding of processes that take place upon sulfur interaction with Fe nanoparticles (Supporting Figure 3). In the sintered sample the Curie temperature is higher than 350 K and there is no specific inception of the magnetization increase at lower temperatures. However, some features are similar, including the magnetization maxima with a rather small magnetization value of less than 0.08 μ_B/Fe, and further decrease of magnetization upon reducing the temperature, which supports the assumption that the dominant response is related to iron sulfide nanostructures in the studied material. Importantly, we detect that magnetization is reduced when the sample is cooled in the presence of magnetic field (Supporting Figure 3b), which is a clear indication of the antiferromagnetic response in the temperature range 150 - 40 K. It seems that the sintered sulfide is composed of pyrite domains with additional surface Fe_xS arrangement.

The general similarity between the magnetization curves of the sintered sample and filled SWCNTs suggests that the encapsulated pyrite nanoparticles contains thin surface layers composed of magnetic low-coordinated iron. The exact configuration should be governed by the diameter of the nanotube, similarly to the case of organosulfur compounds [50,51] or coronene-based molecules [52] inside the nanotubes, where the narrow diameter tubes provide the ordering of molecules stacks [53], while larger diameter nanotubes render the formation of graphene nanoribbons [7,50,54]. As a driving force for the antiferromagnetic ordering one can consider the long-range magneto-dipole interaction between encapsulated pyrite nanoparticles that can be established even between individual filled nanotubes. However, we note that in the systems with the distances between the separated magnetic nanoclusters around 1 nm the exchange interaction becomes strong and should also be taken into account [16,55]. Troilite and recently reported expanded FeS with short range antiferromagnetic order [33] have magnetic moments pointing along the *c*-axis and in the case of formation inside the nanotube moments would be pointing along the tube axis. Another interesting arrangement that was demonstrated inside the nanotubes is the sulfur containing linear polymerized chains [25]. The diameter dependent configurations of these chains, including one, two or three aligned 1D structures, also suggest the possibility for antiferromagnetic ordering. More studies need to be performed in order to corroborate the type of encapsulated structure with the detected magnetic response. Moreover, the presence of nanotube structural defects and remained non-reacted

Fe [38,56,57], both may influence significantly the properties of the material including its magnetic response.

Finally, we demonstrate how the high pressure applied during the annealing of SWCNTs with sulfur affects the magnetic response of the obtained material. Note that HTHP conditions promote liquid-phase filling of SWCNTs, while the HT protocol results in vapor-phase diffusion of sulfur inside nanotubes. According to EDX analysis, the content of sulfur in the HTHP sample is about 37.5 wt%. AAS spectroscopy detected about 0.2 wt% of iron. HR TEM also showed filling of SWCNTs with polymeric chains (indicated by red arrows in Figure 2a), which can be assigned to encapsulated sulfur species. The applied pressure partially breaks the nanotubes shortening them (see inset in Figure 2a) and creating additional structural defects in their walls that correlates with an increase in the ratio of the integrated intensities of D to G peaks in the Raman spectrum (Figure 2b). This is in contrast with the unaffected morphology of SWCNTs filled with sulfur using HT synthesis (Figure 1a and 1b). The Raman spectrum of the pressed sample showed a giant response from the encapsulated sulfur (peaks at *ca*. 319, 394, 645, 714, 788, 1033 and 1100 cm^{-1}), while the ratio of RBM peaks to G peak intensity is close to the values for initial SWCNTs and nanotubes filled without application of pressure. A similar spectrum previously reported for small diameter sulfur-filled HiPCO-SWCNTs was attributed to a strong van der Waals interaction of the confined species with the walls of the nanotubes [41]. We used nanotubes of larger diameter, therefore, the significantly enhanced intensity of the vibrations related to the encapsulated sulfur species suggests a highly dense filling of the SWCNTs cavities under pressure. Unfortunately, these Raman spectral lines hinder the possible response from Fe or iron sulfide particles if they are present. The XRD pattern of the sample does not show any clear fingerprints from phases other than SWCNTs and graphite (Figure 2c).

Turning to the magnetic data, the susceptibility of HTHP-obtained sulfur-filled SWCNTs is significantly (by about an order of magnitude) reduced with respect to that of SWCNTs filled without additional pressure (Figure 2d and 2e). In the magnetization hysteresis measurements (Figure 2f), a saturation around 8 kOe is still visible. However, no clear signature of an antiferromagnetic response is presented. A weak ferromagnetic ordering below 110 K shows up in data taken at H=1 kOe, yet becomes hardly seen at H=10 kOe. We suggest that the ferromagnetic response and the reduced Curie temperature can be explained by the difference in amounts and sizes of the encapsulated magnetic nanostructures. Taking into account the finite-size scaling theory [47] we suppose that larger Fe nanoparticles that participated in the Fe-S structure formation were removed from the nanotube interior under elevated pressure. According to the previous report [58], in the case of encapsulated $FeCp_2$ molecules the diffusion of iron outside the nanotube and its aggregation into nanoparticles can be completed already at 873 K. Liquid sulfur acts as a transport medium promoting extraction of Fe from the cavity through open ends of SWCNTs and defects in the walls created under high pressure. At the same time, sulfur is much less soluble in this carbon rich environment in comparison with iron, explaining the high filling density of sulfur inside the SWCNTs. When iron gets out, it dissolves into high-pressure graphitic cell escaping from the sample. That agrees with the lowering of the iron content and the magnetization value of the HTHP sample compared with the values for initial and HT SWCNTs.

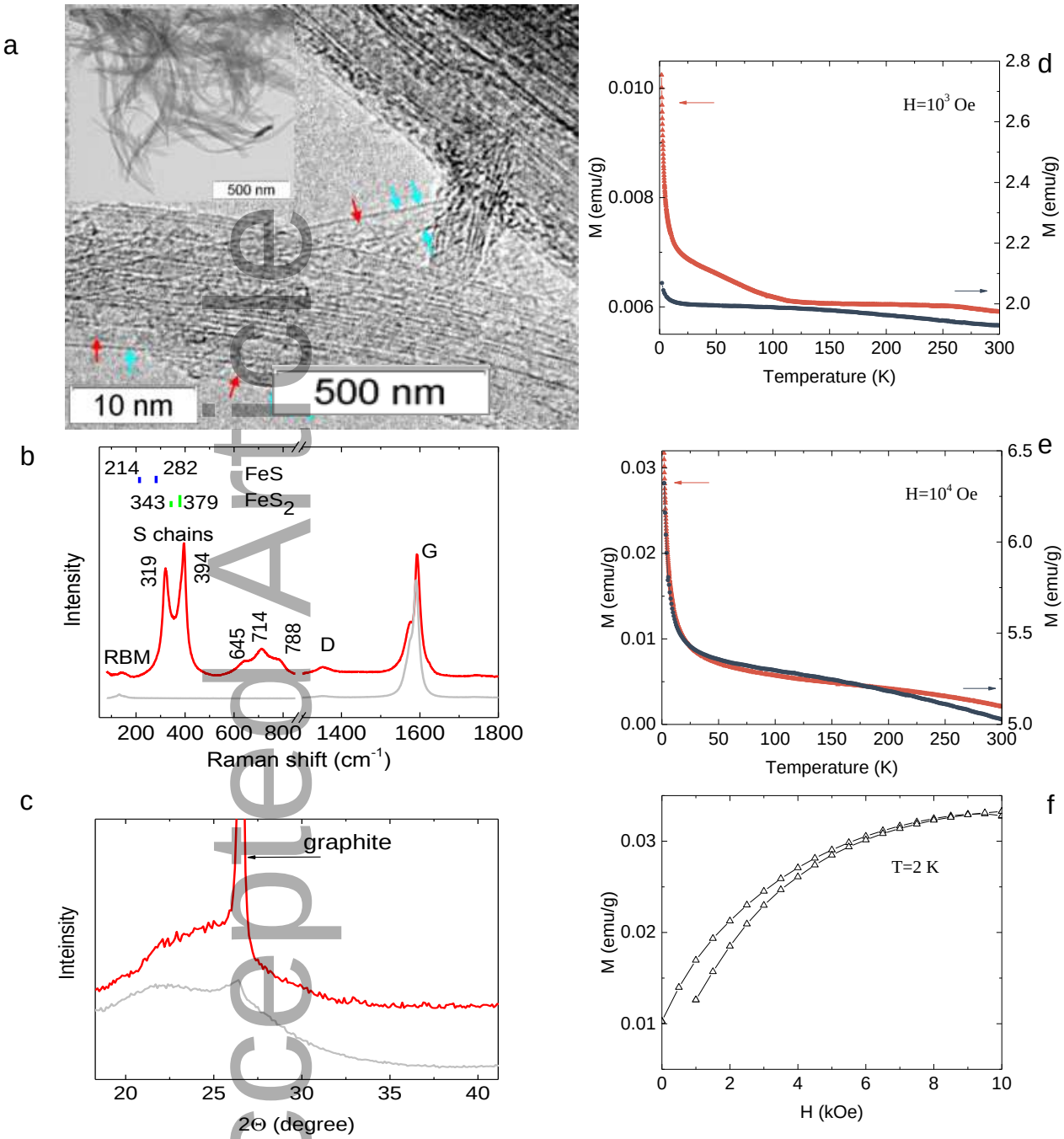

Figure 2. SWCNTs filled with sulfur under HTHP conditions: (a) HR TEM image (cyan and red arrows indicate SWCNTs' walls and sulfur chains), insert shows TEM image, (b) Raman spectra, and (c) XRD patterns for pristine (grey) and sulfur-filled SWCNTs (red). (d) ZFC magnetization data taken at H=1 kOe (e) at H=10 kOe for pristine (grey) and sulfur-filled SWCNTs (red). (f) M (H) measured at 2 K.

To conclude, we examined the magnetic properties of SWCNTs with encapsulated iron sulfide nanoparticles obtained by the reaction of residual encapsulated catalytic species with sulfur at elevated temperatures with and without applied high pressure. The material obtained under merely high temperatures contains predominantly pyrite nanoparticles endowing the host-guest structure with a ferromagnetic-type behavior below 175 K and an antiferromagnetic ordering below ~75 K. Such an unusual magnetic behavior for encapsulated sulfur-based nanomaterial material can be assigned to the presence of Fe_xS nanolayers and to peculiar ordering due to confinement. We suggest that the antiferromagnetic ordering arises from the long-range magneto-dipole interaction between encapsulated nanoparticles through nanotubes walls and from exchange interaction of closely located nanoparticles. HPHT filling brings about a significant increase of the Raman response from encapsulated sulfur that we attribute to the improvement of the filling of SWCNTs cavities, although simultaneously the iron partially diffuses outside the nanotubes. As a result, the filled SWCNTs obtained by HPHT method exhibit a significantly reduced ferromagnetic response related to trace concentrations of Fe that avoided extraction or conversion into non-magnetic state in pyrite nanoparticles. 1D ordered sulfur compounds inside SWCNTs can be used as a new platform for nanoscale magnetophotonic applications. Properties of the encapsulated structures can be governed by the synthesis parameters and diameters of the hosting nanotubes.

Methods

SWCNTs (OCSiAl) with a diameter range of about 1.7–1.9 nm purified from iron [21] and pre-opened were used in this work, which we refer to as pristine. Non-purified ones are called raw in this work. The Fe content in the pristine SWCNTs was estimated to be below 0.3 wt% by AAS [21]. Filling of nanotubes with sulfur was carried out using two approaches: (1) ampoule method described elsewhere [39] and (2) hot pressing [59–61,62]. Briefly, in the first approach mixture of SWCNTs and sulfur with a ratio of 1:4 was heated in a sealed quartz ampoule at 750°C for 1 h and 600°C for 14 h. Hot pressing approach was carried out using a split-sphere multi-anvil apparatus [59]. A mixture of SWCNTs and sulfur taken with ratio 1:2 was embedded into a graphite capsule, which was loaded into a high-pressure cell. The experiments were performed at 5 GPa and temperature of 800°C for 2 h. The products synthesized by the ampoule and pressing method were cleaned in toluene for 10 min using an ultrasound bath to remove the excessive sulfur. For the control experiment, a mixture of iron and sulfur taken with ratio 1:2 was heated in a sealed quartz ampoule at 600°C for 15 h.

The structure of materials was characterized by TEM using a JEOL 2010 microscope and scanning electron microscopy using a JEOL JSM 6700F microscope equipped with an EDX detector (TM-3000). XRD patterns were obtained at room temperature using a Shimadzu XRD-7000 diffractometer (Cu Kα radiation, Ni filter on the reflected beam). In order to decrease the background contribution, the powders were deposited on a zero-diffraction plate of a SiO_2 single-crystal. For XRD measurements, powders of SWCNTs were pressed between graphite foils under 200 atm for 15 min (residual foil gives the intensive XRD peak located at 26.6°). The concentration of iron in the initial and purified samples was quantified by atomic absorption spectroscopy (AAS) on iCAP-6500 (Thermo Scientific, USA) spectrometer with the addition of sample through a pneumatic nebulizer and a cyclone-type spray chamber. Raman analysis was performed at room temperature with a LabRAM HR Evolution spectrometer using a 514 nm excitation. Magnetization data were taken in the temperature range 1.7 – 330 K, at magnetic fields up to 10 kOe using a MPMS-XL SQUID magnetometer. Temperature dependences of the magnetization were measured on heating after cooling the sample in zero magnetic field (ZFC) or after cooling in magnetic field (FC) as well as upon cooling the sample.

Acknowledgments

This research of sulfur-filled SWCNTs obtained under by ampoule synthesis has been funded by the Russian Science Foundation (grant 18-72-00017), magnetic experiments at room temperature were partially performed in terms of RFBR 18-02-01099, high pressure experiments were

performed on state assignment of IGM SB RAS. The authors thank Dr. A.V. Ishchenko for the TEM images.

References

(1) Rafiee, E.; Khodayari, M. Starch as a Green Source for Fe3O4@carbon Core–Shell Nanoparticles Synthesis: A Support for 12-Tungstophosphoric Acid, Synthesis, Characterization, and Application as an Efficient Catalyst. *Res. Chem. Intermed.* **2016**, *42* (4), 3523–3536. https://doi.org/10.1007/s11164-015-2229-5.

(2) del Carmen Giménez-López, M.; Moro, F.; La Torre, A.; Gómez-García, C. J.; Brown, P. D.; van Slageren, J.; Khlobystov, A. N. Encapsulation of Single-Molecule Magnets in Carbon Nanotubes. *Nat. Commun.* **2011**, *2* (1), 407. https://doi.org/10.1038/ncomms1415.

(3) Korneva, G.; Ye, H.; Gogotsi, Y.; Halverson, D.; Friedman, G.; Bradley, J.-C.; Kornev, K. G. Carbon Nanotubes Loaded with Magnetic Particles. *Nano Lett.* **2005**, *5* (5), 879–884. https://doi.org/10.1021/nl0502928.

(4) Khlobystov, A. N. Carbon Nanotubes: From Nano Test Tube to Nano-Reactor. *ACS Nano* **2011**, *5* (12), 9306–9312. https://doi.org/10.1021/nn204596p.

(5) Rybkovskiy, D. V; Impellizzeri, A.; Obraztsova, E. D.; Ewels, C. P. Polyiodide Structures in Thin Single-Walled Carbon Nanotubes: A Large-Scale Density-Functional Study. *Carbon N. Y.* **2019**, *142*, 123–130. https://doi.org/https://doi.org/10.1016/j.carbon.2018.10.049.

(6) Chernov, A.; Havlicek, M.; Jantsch, W.; Rümmeli, M. H.; Bachmatiuk, A.; Yanagi, K.; Peterlik, H.; Kataura, H.; Sauerzopf, F.; Resel, R.; Simon, F.; Kuzmany, H. Ferromagnetic Decoration in Metal–Semiconductor Separated and Ferrocene Functionalized Single-Walled Carbon Nanotubes. *Phys. status solidi* **2012**, *249* (12), 2323–2327. https://doi.org/10.1002/pssb.201200452.

(7) Chernov, A. I.; Fedotov, P. V; Lim, H. E.; Miyata, Y.; Liu, Z.; Sato, K.; Suenaga, K.; Shinohara, H.; Obraztsova, E. D. Band Gap Modification and Photoluminescence Enhancement of Graphene Nanoribbon Filled Single-Walled Carbon Nanotubes. *Nanoscale* **2018**, *10* (6), 2936–2943. https://doi.org/10.1039/C7NR07054C.

(8) Rana, R. K.; Xu, X. N.; Yeshurun, Y.; Gedanken, A. Preparation, Texture, and Magnetic Properties of Carbon Nanotubes/Nanoparticles Doped with Cobalt. *J. Phys. Chem. B* **2002**, *106* (16), 4079–4084. https://doi.org/10.1021/jp013320t.

(9) Che, R. C.; Peng, L.-M.; Duan, X. F.; Chen, Q.; Liang, X. L. Microwave Absorption Enhancement and Complex Permittivity and Permeability of Fe Encapsulated within Carbon Nanotubes. *Adv. Mater.* **2004**, *16* (5), 401–405. https://doi.org/10.1002/adma.200306460.

(10) Zhang, X. X.; Wen, G. H.; Huang, S.; Dai, L.; Gao, R.; Wang, Z. L. Magnetic Properties of Fe Nanoparticles Trapped at the Tips of the Aligned Carbon Nanotubes. *J. Magn. Magn. Mater.* **2001**, *231* (1), 9–12. https://doi.org/https://doi.org/10.1016/S0304-8853(01)00134-2.

(11) Lee, J.-S.; Song, Y.-J.; Hsu, H.-S.; Lin, C.-R.; Huang, J.-Y.; Chen, J. Magnetic Enhancement of Carbon-Encapsulated Magnetite Nanoparticles. *J. Alloys Compd.* **2019**, *790*, 716–722. https://doi.org/https://doi.org/10.1016/j.jallcom.2019.03.191.

(12) Nakanishi, R.; Satoh, J.; Katoh, K.; Zhang, H.; Breedlove, B. K.; Nishijima, M.; Nakanishi, Y.; Omachi, H.; Shinohara, H.; Yamashita, M. DySc2N@C80 Single-Molecule Magnetic Metallofullerene Encapsulated in a Single-Walled Carbon Nanotube. *J. Am. Chem. Soc.* **2018**, *140* (35), 10955–10959. https://doi.org/10.1021/jacs.8b06983.

(13) Katoh, K.; Yamashita, S.; Yasuda, N.; Kitagawa, Y.; Breedlove, B. K.; Nakazawa, Y.; Yamashita, M. Control of the Spin Dynamics of Single-Molecule Magnets by Using a Quasi One-Dimensional Arrangement. *Angew. Chemie Int. Ed.* **2018**, *57* (30), 9262–9267. https://doi.org/10.1002/anie.201803161.

(14) Cleuziou, J.-P.; Wernsdorfer, W.; Ondarçuhu, T.; Monthioux, M. Electrical Detection of Individual Magnetic Nanoparticles Encapsulated in Carbon Nanotubes. *ACS Nano* **2011**, *5* (3), 2348–2355. https://doi.org/10.1021/nn2000349.

(15) Danilyuk, A. L.; Kukharev, A. V; Cojocaru, C. S.; Le Normand, F.; Prischepa, S. L. Impact

of Aligned Carbon Nanotubes Array on the Magnetostatic Isolation of Closely Packed Ferromagnetic Nanoparticles. *Carbon N. Y.* **2018**, *139*, 1104–1116. https://doi.org/https://doi.org/10.1016/j.carbon.2018.08.024.

(16) Iskhakov, R. S.; Komogortsev, S. V; Balaev, A. D.; Okotrub, A. V; Kudashov, A. G.; Kuznetsov, V. L.; Butenko, Y. V. Fe Nanowires in Carbon Nanotubes as an Example of a One-Dimensional System of Exchange-Coupled Ferromagnetic Nanoparticles. *J. Exp. Theor. Phys. Lett.* **2003**, *78* (4), 236–240. https://doi.org/10.1134/1.1622038.

(17) Qi, X.; Xu, J.; Zhong, W.; Au, C.; Du, Y. Controllable Synthesis, Characterization, and Magnetic Properties of Magnetic Nanoparticles Encapsulated in Carbon Nanocages and Carbon Nanotubes. *Diam. Relat. Mater.* **2014**, *45*, 12–19. https://doi.org/https://doi.org/10.1016/j.diamond.2014.02.013.

(18) Zagainova, V. S.; Makarova, T. L.; Okotrub, A. V; Kurenya, A. G.; Komogortsev, S. V; Bulusheva, L. G. Magnetic Properties of Carbon Nanotubes with Low Content of Fe. *Fullerenes, Nanotub. Carbon Nanostructures* **2010**, *18* (4–6), 569–573. https://doi.org/10.1080/1536383X.2010.488082.

(19) Shiozawa, H.; Briones-Leon, A.; Domanov, O.; Zechner, G.; Sato, Y.; Suenaga, K.; Saito, T.; Eisterer, M.; Weschke, E.; Lang, W.; Peterlik, H.; Pichler, T. Nickel Clusters Embedded in Carbon Nanotubes as High Performance Magnets. *Sci. Rep.* **2015**, *5* (1), 15033. https://doi.org/10.1038/srep15033.

(20) He, M.; Jiang, H.; Kauppi, I.; Fedotov, P. V; Chernov, A. I.; Obraztsova, E. D.; Cavalca, F.; Wagner, J. B.; Hansen, T. W.; Sainio, J.; Sairanen, E.; Lehtonen, J.; Kauppinen, E. I. Insights into Chirality Distributions of Single-Walled Carbon Nanotubes Grown on Different CoxMg1−xO Solid Solutions. *J. Mater. Chem. A* **2014**, *2* (16), 5883–5889. https://doi.org/10.1039/C3TA15325H.

(21) Gurova, O. A.; Arhipov, V. E.; Koroteev, V. O.; Guselnikova, T. Y.; Asanov, I. P.; Sedelnikova, O. V; Okotrub, A. V. Purification of Single-Walled Carbon Nanotubes Using Acid Treatment and Magnetic Separation. *Phys. status solidi* **2019**, *256* (9), 1800742. https://doi.org/10.1002/pssb.201800742.

(22) Briones-Leon, A.; Ayala, P.; Liu, X.; Yanagi, K.; Weschke, E.; Eisterer, M.; Jiang, H.; Kataura, H.; Pichler, T.; Shiozawa, H. Orbital and Spin Magnetic Moments of Transforming One-Dimensional Iron inside Metallic and Semiconducting Carbon Nanotubes. *Phys. Rev. B* **2013**, *87* (19), 195435. https://doi.org/10.1103/PhysRevB.87.195435.

(23) Havlicek, M.; Chernov, A.; Jantsch, W.; Wilamowski, Z.; Yanagi, K.; Kataura, H.; Rümmeli, M. H.; Malissa, H.; Kuzmany, H. Magnetic Phase Transition for Defect Induced Electron Spins from Fully Metal–Semiconductor Separated SWCNTs. *Phys. status solidi* **2012**, *249* (12), 2562–2567. https://doi.org/10.1002/pssb.201200426.

(24) Havlicek, M.; Jantsch, W.; Wilamowski, Z.; Yanagi, K.; Kataura, H.; Rümmeli, M. H.; Malissa, H.; Tyryshkin, A.; Lyon, S.; Chernov, A.; Kuzmany, H. Indirect Exchange Interaction in Fully Metal-Semiconductor Separated Single-Walled Carbon Nanotubes Revealed by Electron Spin Resonance. *Phys. Rev. B* **2012**, *86* (4), 45402. https://doi.org/10.1103/PhysRevB.86.045402.

(25) Fujimori, T.; Morelos-Gómez, A.; Zhu, Z.; Muramatsu, H.; Futamura, R.; Urita, K.; Terrones, M.; Hayashi, T.; Endo, M.; Young Hong, S.; Chul Choi, Y.; Tománek, D.; Kaneko, K. Conducting Linear Chains of Sulphur inside Carbon Nanotubes. *Nat. Commun.* **2013**, *4* (1), 2162. https://doi.org/10.1038/ncomms3162.

(26) Fu, C.; Oviedo, M. B.; Zhu, Y.; von Wald Cresce, A.; Xu, K.; Li, G.; Itkis, M. E.; Haddon, R. C.; Chi, M.; Han, Y.; Wong, B. M.; Guo, J. Confined Lithium–Sulfur Reactions in Narrow-Diameter Carbon Nanotubes Reveal Enhanced Electrochemical Reactivity. *ACS Nano* **2018**, *12* (10), 9775–9784. https://doi.org/10.1021/acsnano.7b08778.

(27) Cabán-Acevedo, M.; Faber, M. S.; Tan, Y.; Hamers, R. J.; Jin, S. Synthesis and Properties of Semiconducting Iron Pyrite (FeS2) Nanowires. *Nano Lett.* **2012**, *12* (4), 1977–1982. https://doi.org/10.1021/nl2045364.

(28) Zhu, Y.; Fan, X.; Suo, L.; Luo, C.; Gao, T.; Wang, C. Electrospun FeS2@Carbon Fiber Electrode as a High Energy Density Cathode for Rechargeable Lithium Batteries. *ACS Nano* **2016**, *10* (1), 1529–1538. https://doi.org/10.1021/acsnano.5b07081.
(29) Xu, L.; Hu, Y.; Zhang, H.; Jiang, H.; Li, C. Confined Synthesis of FeS2 Nanoparticles Encapsulated in Carbon Nanotube Hybrids for Ultrastable Lithium-Ion Batteries. *ACS Sustain. Chem. Eng.* **2016**, *4* (8), 4251–4255. https://doi.org/10.1021/acssuschemeng.6b00741.
(30) Fan, M.; Zhang, L.; Li, K.; Liu, J.; Zheng, Y.; Zhang, L.; Song, S.; Qiao, Z.-A. FeS2@C Core–Shell Nanochains as Efficient Electrocatalysts for Hydrogen Evolution Reaction. *ACS Appl. Nano Mater.* **2019**, *2* (6), 3889–3896. https://doi.org/10.1021/acsanm.9b00736.
(31) Burgardt, P.; Seehra, M. S. Magnetic Susceptibility of Iron Pyrite (FeS2) between 4.2 and 620 K. *Solid State Commun.* **1977**, *22* (2), 153–156. https://doi.org/https://doi.org/10.1016/0038-1098(77)90422-7.
(32) Adachi, K.; Sato, K. Origin of Magnetic Anisotropy Energy of Fe7S8 and Fe7Se8. *J. Appl. Phys.* **1968**, *39* (2), 1343–1344. https://doi.org/10.1063/1.1656293.
(33) Wang, M.; Yi, M.; Frandsen, B. A.; Yin, J.; Sun, H.; Xu, Z.; Cao, H.; Bourret-Courchesne, E.; Lynn, J. W.; Birgeneau, R. J. Observation of a C-Type Short-Range Antiferromagnetic Order in Layer Spacing Expanded FeS. *Phys. Rev. Mater.* **2020**, *4* (3), 34802. https://doi.org/10.1103/PhysRevMaterials.4.034802.
(34) Powell, A. V; Vaqueiro, P.; Knight, K. S.; Chapon, L. C.; Sánchez, R. D. Structure and Magnetism in Synthetic Pyrrhotite ${\text{Fe}}_{7}{\mathrm{S}}_{8}$: A Powder Neutron-Diffraction Study. *Phys. Rev. B* **2004**, *70* (1), 14415. https://doi.org/10.1103/PhysRevB.70.014415.
(35) Roberts, A. P. Magnetic Properties of Sedimentary Greigite (Fe3S4). *Earth Planet. Sci. Lett.* **1995**, *134* (3), 227–236. https://doi.org/https://doi.org/10.1016/0012-821X(95)00131-U.
(36) Limpinsel, M.; Farhi, N.; Berry, N.; Lindemuth, J.; Perkins, C. L.; Lin, Q.; Law, M. An Inversion Layer at the Surface of N-Type Iron Pyrite. *Energy Environ. Sci.* **2014**, *7* (6), 1974–1989. https://doi.org/10.1039/C3EE43169J.
(37) Apostolov, A. T.; Apostolova, I. N.; Trimper, S.; Wesselinowa, J. M. Origin of Ferromagnetism in Pure and Ion Doped Pyrite FeS2 Nanoparticles. *Phys. status solidi* **2019**, *256* (10), 1900201. https://doi.org/10.1002/pssb.201900201.
(38) Xia, J.; Jiao, J.; Dai, B.; Qiu, W.; He, S.; Qiu, W.; Shen, P.; Chen, L. Facile Synthesis of FeS2 Nanocrystals and Their Magnetic and Electrochemical Properties. *RSC Adv.* **2013**, *3* (17), 6132–6140. https://doi.org/10.1039/C3RA22405H.
(39) Sedelnikova, O.V.; Gurova, O.A.; Makarova, A.A.; Fedorenko, A.D.; Nikolenko, A.D.; Plyusnin, P.E.; Arenal, R.; Bulusheva, L.G.; Okotrub, A. V. Light-Induced Sulfur Transport inside Single-Walled Carbon Nanotubes. *Nanomaterials* **2020**, *10* (5), 818.
(40) Kissin, S. A.; Scott, S. D. Phase Relations Involving Pyrrhotite below 350 Degrees C. *Econ. Geol.* **1982**, *77* (7), 1739–1754. https://doi.org/10.2113/gsecongeo.77.7.1739.
(41) Li, G.; Fu, C.; Oviedo, M. B.; Chen, M.; Tian, X.; Bekyarova, E.; Itkis, M. E.; Wong, B. M.; Guo, J.; Haddon, R. C. Giant Raman Response to the Encapsulation of Sulfur in Narrow Diameter Single-Walled Carbon Nanotubes. *J. Am. Chem. Soc.* **2016**, *138* (1), 40–43. https://doi.org/10.1021/jacs.5b10598.
(42) Baum, A.; Milosavljević, A.; Lazarević, N.; Radonjić, M. M.; Nikolić, B.; Mitschek, M.; Maranloo, Z. I.; Šćepanović, M.; Grujić-Brojčin, M.; Stojilović, N.; Opel, M.; Wang, A.; Petrovic, C.; Popović, Z. V; Hackl, R. Phonon Anomalies in FeS. *Phys. Rev. B* **2018**, *97* (5), 54306. https://doi.org/10.1103/PhysRevB.97.054306.
(43) Boughriet, A.; Figueiredo, R. S.; Laureyns, J.; Recourt, P. Identification of Newly Generated Iron Phases in Recent Anoxic Sediments: 57Fe Mössbauer and MicroRaman Spectroscopic Studies. *J. Chem. Soc. Faraday Trans.* **1997**, *93* (17), 3209–3215. https://doi.org/10.1039/A701068K.
(44) Vogt, H.; Chattopadhyay, T.; Stolz, H. J. Complete First-Order Raman Spectra of the Pyrite

Structure Compounds FeS2, MnS2 AND SiP2. *J. Phys. Chem. Solids* **1983**, *44* (9), 869–873. https://doi.org/https://doi.org/10.1016/0022-3697(83)90124-5.
(45) Cui, W.; Saito, T.; Ayala, P.; Pichler, T.; Shi, L. Oxidation Stability of Confined Linear Carbon Chains, Carbon Nanotubes, and Graphene Nanoribbons as 1D Nanocarbons. *Nanoscale* **2019**, *11* (32), 15253–15258. https://doi.org/10.1039/C9NR04924J.
(46) Borowiak-Palen, E.; Mendoza, E.; Bachmatiuk, A.; Rummeli, M. H.; Gemming, T.; Nogues, J.; Skumryev, V.; Kalenczuk, R. J.; Pichler, T.; Silva, S. R. P. Iron Filled Single-Wall Carbon Nanotubes – A Novel Ferromagnetic Medium. *Chem. Phys. Lett.* **2006**, *421* (1), 129–133. https://doi.org/https://doi.org/10.1016/j.cplett.2006.01.072.
(47) Rong, C. -b.; Li, D.; Nandwana, V.; Poudyal, N.; Ding, Y.; Wang, Z. L.; Zeng, H.; Liu, J. P. Size-Dependent Chemical and Magnetic Ordering in L10-FePt Nanoparticles. *Adv. Mater.* **2006**, *18* (22), 2984–2988. https://doi.org/10.1002/adma.200601904.
(48) Cowburn, R. P.; Koltsov, D. K.; Adeyeye, A. O.; Welland, M. E.; Tricker, D. M. Single-Domain Circular Nanomagnets. *Phys. Rev. Lett.* **1999**, *83* (5), 1042–1045. https://doi.org/10.1103/PhysRevLett.83.1042.
(49) Gélvez, C. F.; Patiño, E. J. Coercive Field Enhancement in Co Nanodisks: Single-Domain to Vortex Switching. *J. Phys. Condens. Matter* **2019**, *31* (13), 13LT01. https://doi.org/10.1088/1361-648x/ab015e.
(50) Chamberlain, T. W.; Biskupek, J.; Rance, G. A.; Chuvilin, A.; Alexander, T. J.; Bichoutskaia, E.; Kaiser, U.; Khlobystov, A. N. Size, Structure, and Helical Twist of Graphene Nanoribbons Controlled by Confinement in Carbon Nanotubes. *ACS Nano* **2012**, *6* (5), 3943–3953. https://doi.org/10.1021/nn300137j.
(51) Miyaura, K.; Miyata, Y.; Thendie, B.; Yanagi, K.; Kitaura, R.; Yamamoto, Y.; Arai, S.; Kataura, H.; Shinohara, H. Extended-Conjugation π-Electron Systems in Carbon Nanotubes. *Sci. Rep.* **2018**, *8* (1), 8098. https://doi.org/10.1038/s41598-018-26379-4.
(52) Anoshkin, I. V; Talyzin, A. V; Nasibulin, A. G.; Krasheninnikov, A. V; Jiang, H.; Nieminen, R. M.; Kauppinen, E. I. Coronene Encapsulation in Single-Walled Carbon Nanotubes: Stacked Columns, Peapods, and Nanoribbons. *ChemPhysChem* **2014**, *15* (8), 1660–1665. https://doi.org/10.1002/cphc.201301200.
(53) Chernov, A. I.; Fedotov, P. V.; Anoshkin, I. V.; Nasibulin, A. G.; Kauppinen, E. I.; Kuznetsov, V. L.; Obraztsova, E. D. Single-Walled Carbon Nanotubes as a Template for Coronene Stack Formation. *Phys. Status Solidi Basic Res.* **2014**, *251* (12), 2372–2377. https://doi.org/10.1002/pssb.201451159.
(54) Chuvilin, A.; Bichoutskaia, E.; Gimenez-Lopez, M. C.; Chamberlain, T. W.; Rance, G. A.; Kuganathan, N.; Biskupek, J.; Kaiser, U.; Khlobystov, A. N. Self-Assembly of a Sulphur-Terminated Graphene Nanoribbon within a Single-Walled Carbon Nanotube. *Nat. Mater.* **2011**, *10* (9), 687–692. https://doi.org/10.1038/nmat3082.
(55) Bedanta, S.; Eimüller, T.; Kleemann, W.; Rhensius, J.; Stromberg, F.; Amaladass, E.; Cardoso, S.; Freitas, P. P. Overcoming the Dipolar Disorder in Dense CoFe Nanoparticle Ensembles: Superferromagnetism. *Phys. Rev. Lett.* **2007**, *98* (17), 176601. https://doi.org/10.1103/PhysRevLett.98.176601.
(56) Zhang, X.; Scott, T.; Socha, T.; Nielsen, D.; Manno, M.; Johnson, M.; Yan, Y.; Losovyj, Y.; Dowben, P.; Aydil, E. S.; Leighton, C. Phase Stability and Stoichiometry in Thin Film Iron Pyrite: Impact on Electronic Transport Properties. *ACS Appl. Mater. Interfaces* **2015**, *7* (25), 14130–14139. https://doi.org/10.1021/acsami.5b03422.
(57) Roberts, D. M.; Russek, S. E.; Stoldt, C. R. Synthetic Iron Pyrite across Length Scales: Interfacial Defects and Macroscopic Properties. *CrystEngComm* **2019**, *21* (21), 3304–3312. https://doi.org/10.1039/C9CE00145J.
(58) Shiozawa, H.; Pichler, T.; Grüneis, A.; Pfeiffer, R.; Kuzmany, H.; Liu, Z.; Suenaga, K.; Kataura, H. A Catalytic Reaction Inside a Single-Walled Carbon Nanotube. *Adv. Mater.* **2008**, *20* (8), 1443–1449. https://doi.org/10.1002/adma.200701466.
(59) Pal'yanov, Yu.N., Khokhryakov, A.F., Borzdov, Yu.M., Sokol, A.G., Gusev, V.A., Rylov,

G.M., Sobolev, N. V. Growth Conditions and Real Structure of Synthetic Diamond Crystals. *Geol. i Geofiz. (Russian Geol. Geophys.* **1997**, *38* (5), 882–906 (920–945).
(60) Palyanov, Y. N.; Borzdov, Y. M.; Kupriyanov, I. N.; Khokhryakov, A. F. Effect of H2O on Diamond Crystal Growth in Metal–Carbon Systems. *Cryst. Growth Des.* **2012**, *12* (11), 5571–5578. https://doi.org/10.1021/cg301111g.
(61) Fedoseeva, Y. V.; Okotrub, A. V; Koroteev, V. O.; Borzdov, Y. M.; Palyanov, Y. N.; Shubin, Y. V.; Maksimovskiy, E. A.; Makarova, A. A.; Münchgesang, W.; Bulusheva, L. G.; Vyalikh, A. Graphitization of 13C Enriched Fine-Grained Graphitic Material under High-Pressure Annealing. *Carbon N. Y.* **2019**, *141*, 323–330. https://doi.org/https://doi.org/10.1016/j.carbon.2018.09.065.
(62) Palyanov, Yu. N.; Kupriyanov, I. N.; Borzdov, Yu. M.; Sokol, A. G.; Khokhryakov, A. F. Diamond Crystallization from a Sulfur-Carbon System at HPHT Conditions. *Cryst. Growth Des.* **2009**, *9 (6)*, 2922-2926. https://doi.org/10.1021/cg900265c.

Supporting information

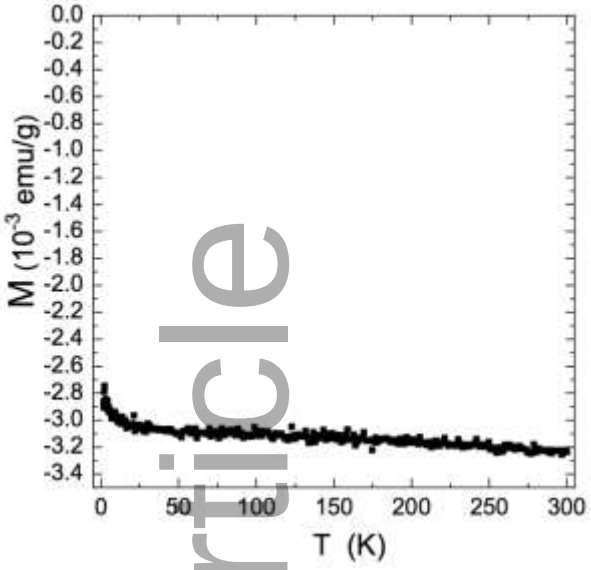

Supporting Figure 1. Magnetic properties of pristine sulfur measured at 10 kOe.

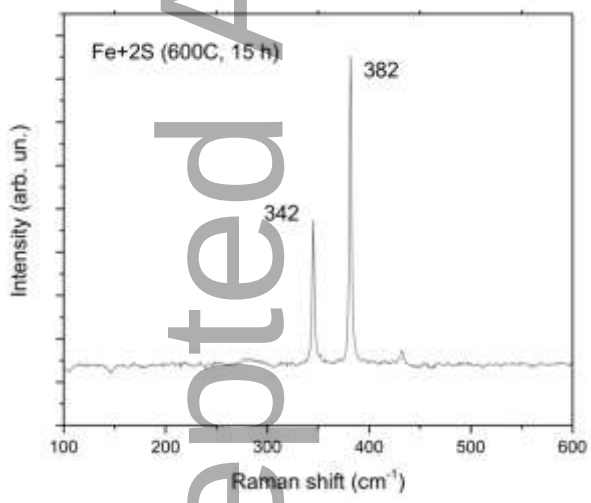

Supporting Figure 2. Raman spectrum of iron sulfide sintered in an ampoule at 600°C for 15 h.

a b c

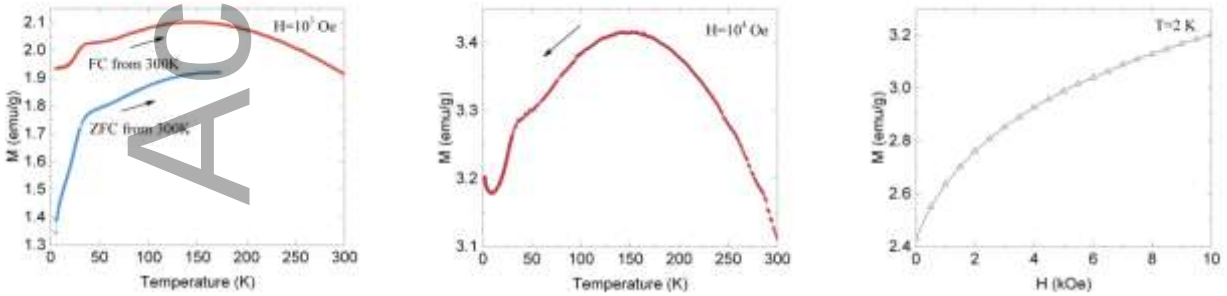

Supporting Figure 3. Magnetic properties after sintering iron with sulfur without nanotubes
(a) ZFC and FC magnetization data at H=1 kOe. (b) Magnetization data taken upon cooling in magnetic field H=10 kOe. (c) M(H) data measured at 2 K revealing apparent remnant magnetization.

TOC

Filling of SWCNTs containing encapsulated iron nanoparticles with sulfur results in the formation of one-dimensional iron sulfide nanoparticles, which demonstrate sequential ferromagnetic-antiferromagnetic ordering. The addition of high pressure treatment results in the partial extraction of iron from SWCNTs' cavities and reduction of the magnetic susceptibility of the material.